This article has been accepted for publication in a future issue of this journal, but has not been fully edited. Content may change prior to final publication. Citation information: DOI 10.1109/TAP.2017.2760360, IEEE Transactions on Antennas and Propagation

A Novel 60 GHz Wideband Coupled Half-Mode/Quarter-Mode Substrate Integrated Waveguide Antenna

Thomas Deckmyn, *Student Member, IEEE*, Sam Agneessens, *Member, IEEE*, Ad C.F. Reniers, A. Bart Smolders, *Senior Member, IEEE,* Maarten Cauwe*, Member, IEEE,* Dries Vande Ginste, *Senior Member, IEEE,* and Hendrik Rogier, *Senior Member, IEEE*

***Abstract*—A novel wideband substrate integrated waveguide (SIW) antenna topology, consisting of coupled half-mode and quarter-mode SIW resonant cavities, is proposed for operation in the 60 GHz band. This innovative topology combines a considerable bandwidth enhancement and a low form factor with compatibility with low-cost PCB manufacturing processes, making it excellently suited for next generation, high data rate wireless applications. Moreover, exploiting SIW technology, a high antenna-platform isolation is obtained, enabling dense integration with active electronics without harmful coupling. The computer-aided design process yields an antenna that covers the entire [57-64] GHz IEEE 802.11ad band with a measured fractional impedance bandwidth of 11.7% (7 GHz). The measured maximum gain and radiation efficiency of the prototype are larger than 5.1 dBi and 65%, respectively, within the entire impedance bandwidth.**

***Index Terms*—Coupled resonators, substrate integrated waveguide (SIW) antenna, half-mode SIW (HMSIW), quarter-mode SIW (QMSIW), bandwidth enhancement, wideband, 60 GHz.**

I. Introduction

In recent years, an increasing demand for broadband multimedia applications has appeared, which forces the capacity of wireless networks to increase continuously. 5G mobile communication is an excellent example of this trend, as extremely high data rates need to be offered to the end user. To this end, novel wideband antenna topologies need to be developed, exhibiting a limited footprint while being implemented through cost-efficient manufacturing, as required for integration into user equipment, such as handsets.

As the spectrum up to 6 GHz is becoming ever more crowded, the [57-64] GHz IEEE 802.11ad band is the ideal candidate to meet the requirements of 5G mobile communication systems, both in terms of bandwidth and number of interconnected devices. This globally available and unlicensed band offers 7 GHz of frequency spectrum for wideband communication. The high atmospheric attenuation, caused by the absorption peak of oxygen atoms, makes the conditions ideal for short range, low interference, and highly secure communication between many devices sharing the same spectrum [1]-[2].

Nowadays, a breakthrough of the very promising Substrate Integrated Waveguide (SIW) technology is apparent in the millimeter wave research field [3]. Recent trends and applications include antennas, filters and couplers for RF front-ends [4], beam steering [5] and MIMO systems [6]. The heightened interest in SIW technology for millimeter wave applications can be attributed to its excellent loss performance, isolation characteristics, and compatibility with standard printed circuit board (PCB) fabrication technology. The electromagnetic fields are confined inside the SIW structure, which suppresses the propagation of surface waves, as such significantly reducing the substrate loss. Moreover, the excellent shielding properties enable the integration of active components in close proximity to the SIW structure [7]-[11], which is of prime interest for the development of extremely high-frequency active antenna systems.

Another tendency is the vast miniaturization of microwave components, and antennas in particular, to arrive at compact, lightweight and easy-to-integrate wireless systems [12]-[13], e.g., for integration in 5G end user equipment. Nevertheless, miniaturization should not invoke a trade-off with the functionality of the device, as is often the case for antennas; excellent performance should be pursued as a top priority.

A rectangular SIW resonant cavity can be miniaturized by bisecting it along fictitious quasi-magnetic walls, as such arriving at half-mode (HMSIW) and quarter-mode (QMSIW) SIW topologies, which correspond to a half and quarter sector of a traditional rectangular SIW cavity, respectively. This miniaturization technique almost completely preserves the field distribution of the original SIW. Moreover, it has been proven

T. Deckmyn, D. Vande Ginste and H. Rogier are with the Department of Information Technology, IDLab, Ghent University – imec, Technologiepark 15, 9052 Ghent, Belgium (e-mail: thomas.deckmyn@intec.ugent.be; dries.vande.ginste@intec.ugent.be; hendrik.rogier@intec.ugent.be).

S. Agneessens is with the Department of Information Technology, IDLab, Ghent University - imec, 9052 Ghent, Belgium, and also with the Centre for Microsystems Technology (CMST), imec and Ghent University, Technologiepark 15, 9052 Ghent, Belgium. He is currently an FWO Postdoctoral Research Fellow with the Research Foundation Flanders, Brussel 1000, Belgium (e-mail: sam.agneessens@intec.ugent.be).

M. Cauwe is with the Centre for Microsystems Technology (CMST), imec and Ghent University, Technologiepark 15, 9052 Ghent, Belgium (e-mail: maarten.cauwe@imec.be).

A. C. F. Reniers and A. B. Smolders are with the Faculty of Electrical Engineering, Eindhoven University of Technology, Eindhoven 5600 MB, The Netherlands (e-mail: a.reniers@tue.nl; a.b.smolders@tue.nl).

that HM- and QMSIWs exhibit excellent microwave performance [14]-[15].

In this paper, a novel wideband SIW antenna topology is proposed. An innovative bandwidth enhancement technique based on three coupled, miniaturized resonators/antennas is exploited, while maintaining a low form factor and compatibility with standard, low-cost PCB processing. Wideband behavior is obtained by skillfully distributing the resonances of the resulting coupled resonators over the frequency range of interest. Taking all of the above into account, the proposed topology is a good candidate for integration in 5G end user equipment. The large bandwidth allows for high data rate communication, while the small footprint facilitates easy integration into small user equipment, such as mobile handsets. Moreover, the compatibility to standard PCB processes enables cost-efficient manufacturing.

Up to now, SIW antenna designs proposed in literature for the 60 GHz band inevitably had to make a trade-off to provide sufficient bandwidth. SIW slot arrays have proven to achieve high bandwidths, but have considerably large form factors [16]-[17]. Low temperature co-fired ceramic (LTCC) and multi-layer PCB technology have been exploited to implement thick substrates [18]-[21] or air cavities [22]-[23], yet the high manufacturing cost and complexity are major drawbacks when considering the targeted 5G end user equipment use case.

Stacked patch topologies have proven to achieve large impedance bandwidths [24]-[25], but do not exhibit high antenna/platform isolation, making an SIW topology a more viable option from an integration point-of-view. An SIW cavity-backed wide slot antenna, based on a *resonant* slot radiation mechanism, is proposed in [26]. In contrast, this work introduces an innovative coupled HMSIW/QMSIW topology, relying on *non-resonant* slots. The flexible and straightforward GCPW feeding technique enables compact antenna array topologies, as opposed to the rather bulky waveguide feed. The thorough analysis of the parameter sensitivity and manufacturing process, performed in Section III, ensures optimal agreement between simulation and measurement.

This paper is organized as follows. In Section II, the novel antenna topology is proposed and the design evolution is discussed. Section III covers manufacturing tolerances, material characterization and a thorough corner-analysis. The fabricated prototype is validated in Section IV. Conclusions and an outlook on future research are presented in Section V.

II. Antenna Design

A. Wideband Operation through Coupled Cavities

The miniaturization technique, briefly discussed above, is improved and exploited to arrive at a novel wideband SIW antenna topology. One HMSIW and two QMSIW cavities are combined to construct a single antenna element, as depicted in Fig. 1. Essentially, this novel topology integrates three separate antenna elements into the footprint of a conventional half wavelength SIW antenna, yielding a considerable improvement in terms of form factor.

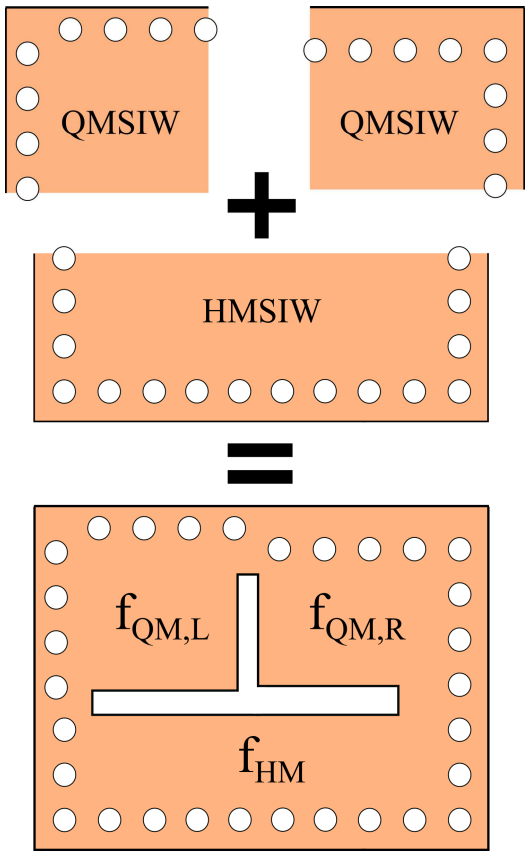

Fig. 1: Construction of the novel antenna topology: one half-mode (HMSIW) and two quarter-mode (QMSIW) SIW cavities are combined into a single antenna element, yielding a considerable bandwidth enhancement.

Each miniaturized cavity in Fig. 1 exhibits a fundamental resonant frequency, calculated by

$$f_{101,HM} = \frac{c}{\sqrt{2\pi\varepsilon_{r,eff}}}\sqrt{\left(\frac{\pi}{W_{eff,HM}}\right)^2 + \left(\frac{\pi}{2L_{eff,HM}}\right)^2} \quad (1)$$

for the HMSIW, and

$$f_{101,QM} = \frac{c}{\sqrt{2\pi\varepsilon_{r,eff}}}\sqrt{\left(\frac{\pi}{2W_{eff,QM}}\right)^2 + \left(\frac{\pi}{2L_{eff,QM}}\right)^2} \quad (2)$$

for the QMSIWs, where W_{eff} and L_{eff} are the effective width and length of the resonant cavities, respectively, and $\varepsilon_{r,eff}$ is the effective relative permittivity of the substrate material. The effective width and length are derived from the equivalence of SIWs with conventional rectangular waveguides. They are given by

$$\begin{cases} W_{eff} = W - \dfrac{d^2}{0.95s} \\ L_{eff} = L - \dfrac{d^2}{0.95s} \end{cases}, \quad (3)$$

where W and L are the physical width and length of the SIW, respectively, and d is the diameter and s the spacing between

This article has been accepted for publication in a future issue of this journal, but has not been fully edited. Content may change prior to final publication. Citation information: DOI 10.1109/TAP.2017.2760360, IEEE Transactions on Antennas and Propagation

the vias. Design guidelines [3] restrict the via diameter d and spacing s to

$$\begin{cases} d \leq \frac{\lambda}{10} \\ s \leq 2d \end{cases}, \tag{4}$$

with λ the wavelength at the frequency of interest. This prevents lateral radiation leakage through the via rows, yielding optimal antenna-platform isolation.

When the HMSIW and QMSIW resonators are brought in close proximity, mode bifurcation due to the coupled resonating cavities occurs. As such, the entire system, consisting of one HMSIW and two QMSIWs, exhibits three distinct cavity resonances that are determined by the dimensions of the miniaturized cavities and the amount of coupling between them.

In our proposed topology, the HMSIW serves as the feeding cavity whereas the QMSIWs are parasitic, i.e. only the HMSIW is excited by an external feed. As a consequence of the strong coupling, the QMSIWs are, in turn, excited by the HMSIW. The antenna radiates via the inverted T-slot separating the miniaturized SIW cavities, as depicted in Fig. 1.

By carefully tuning the dimensions of the HMSIW and QMSIWs and optimizing the coupling between them, the distinct resonance frequencies can be brought close to each other. First, the dimensions of the miniaturized SIW cavities are determined from (1) and (2), to obtain cavity resonances in the desired frequency range. The actual fine-tuning is performed in the second step, during which the dimensions of the slots, separating the cavities, are optimized to carefully control the coupling, yielding an optimal distribution of the resonances within the frequency range of interest. Distributing the three distinct resonances over the frequency range of interest considerably enhances the bandwidth of the antenna. Furthermore, by exploiting the SIW miniaturization technique, three significantly smaller radiating elements are combined into a single antenna with dimensions in the order of half a wavelength, and this without any loss in performance. The fact that both bandwidth and form factor are considerably improved, without any trade-off, represents one of the prime novelties of the coupled HM- and QMSIW antenna topology.

B. Design Procedure

The first step in the design process consists in conceiving the feeding HMSIW cavity in a single layer Rogers 4350B high-frequency laminate, as shown in Fig. 2. Its dimensions are determined using (1), yielding its desired resonant frequency f_{HM}. The HMSIW cavity is excited by a grounded coplanar waveguide (GCPW) transmission line, with insets to tune the impedance matching. This configuration is optimized through full-wave simulations using CST Microwave Studio [27]. The simulated reflection coefficient and electric field are presented in Fig. 3 and Fig. 4, respectively. The half-mode cavity exhibits a clear resonance peak, as expected.

The distribution of the electric field, depicted in Fig. 4, is approximately equal to half the field distribution of a TE_{101}-mode in a full rectangular SIW cavity, justifying the applied miniaturization technique. The fractional bandwidth, for which the $|S_{11}|$ remains below -10 dB, of the single resonance is 4.2%.

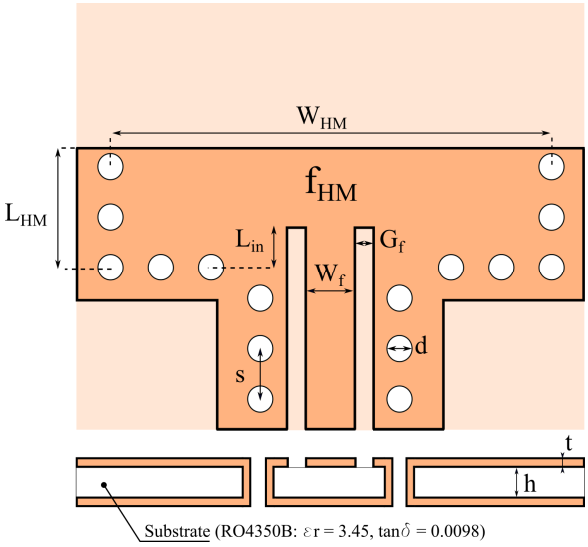

Fig. 2: HMSIW feeding cavity excited by a GCPW transmission line, with insets for impedance matching (W_{HM} = 1.74 mm, L_{HM} = 0.70 mm, L_{in} = 0.06 mm, W_f = 0.42 mm, G_f = 0.10 mm, s = 0.40 mm, d = 0.25 mm, h = 0.50 mm and t = 0.03 mm).

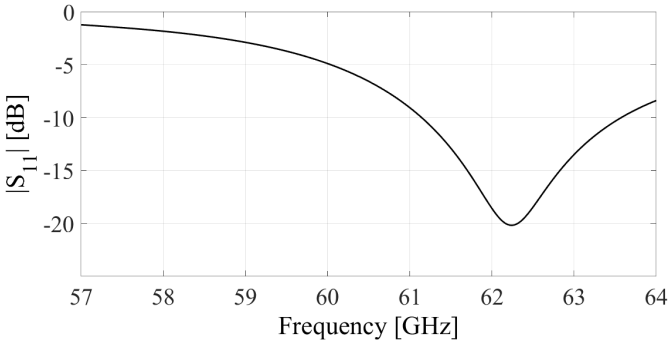

Fig. 3: Simulated reflection coefficient of the HMSIW feeding cavity.

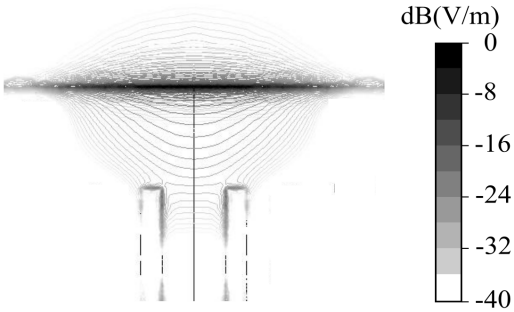

Fig. 4: Simulated normalized electric field distribution inside the HMSIW feeding cavity at 62.2 GHz. (For clarity of the figure, the vias are not shown.)

The next step consists of coupling a QMSIW cavity to the HMSIW feeding cavity, as shown in Fig. 5, yielding an antenna with two resonant modes. The simulated reflection coefficient in Fig. 6 clearly shows two resonance peaks. By carefully optimizing the coupling between both cavities, the resonances are positioned within the desired frequency range, achieving bandwidth enhancement compared to the single half-mode SIW

cavity of Fig. 2. The fractional bandwidth now increases to 6.6%, whereas it was 4.2% for the single resonating cavity.

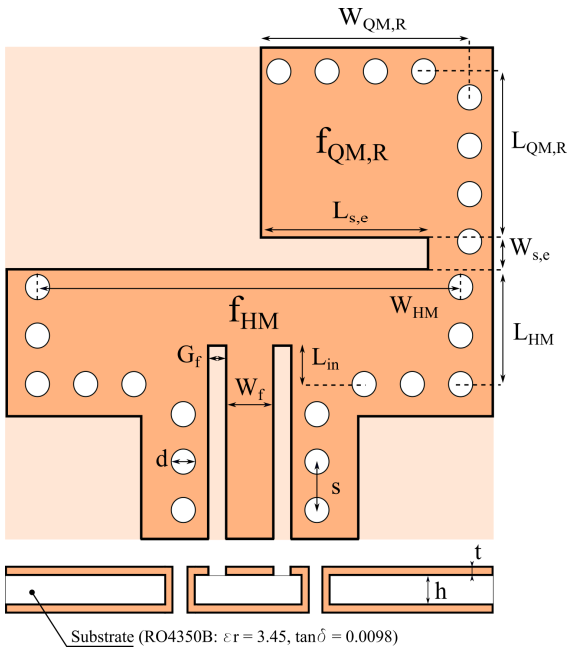

Fig. 5: Parasitic QMSIW cavity coupled to the feeding HMSIW cavity (W_{HM} = 1.84 mm, L_{HM} = 0.70 mm, $W_{QM,R}$ = 1 mm, $L_{QM,R}$ = 0.85 mm, $W_{s,e}$ = 0.3 mm, $L_{s,e}$ = 0.70 mm, L_{in} = 0.06 mm, W_f = 0.42 mm, G_f = 0.10 mm, s = 0.40 mm, d = 0.25 mm, h = 0.50 mm and t = 0.03 mm).

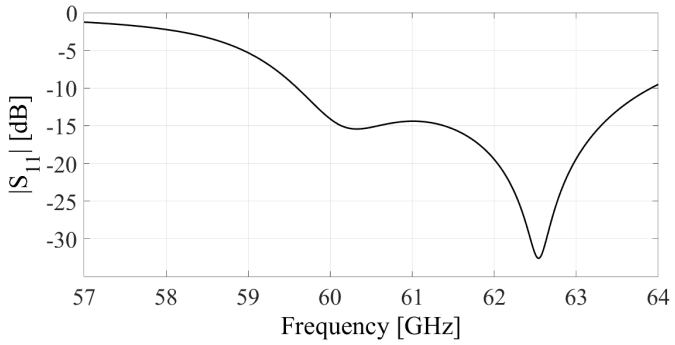

Fig. 6: Simulated reflection coefficient of one parasitic QMSIW cavity coupled to the HMSIW feeding cavity: two distinct resonance peaks.

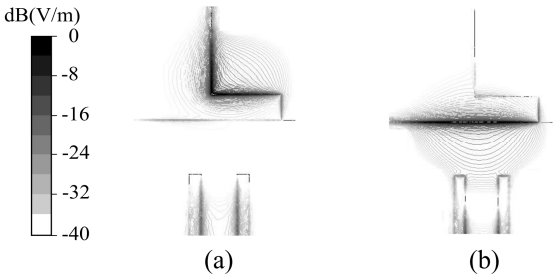

Fig. 1: Simulated normalized electric field distribution in the HMSIW feeding cavity coupled to one parasitic QMSIW: (a) 60.2 GHz, (b) 62.5 GHz. (For clarity of the figure, the vias are not shown.)

The electric field distribution at both resonance frequencies is presented in Fig. 7. These field patterns clearly show that the resonant mode in the QMSIW is dominant at 60.2 GHz, and the mode in the HMSIW dominates at 62.5 GHz. Moreover, the distribution of the field in the QMSIW at 60.2 GHz is approximately equal to a quadrant of the electric field pattern of a TE_{101}-mode in a full rectangular SIW cavity.

In the last design step, the second QMSIW cavity is added, as such arriving at the final coupled HMSIW and QMSIW wideband antenna topology, presented in Fig. 8, with dimensions summarized in Table I.

The simulated reflection coefficient in Fig. 9 now exhibits three distinct resonances, distributed over the desired operating frequency band by tuning the coupling to achieve wideband behavior. The first resonance is attributed to the top left QMSIW, whereas the second resonance is related to the top right QMSIW cavity. The HMSIW is responsible for the highest resonance frequency. The novel coupled HM- and QMSIW antenna covers the entire unlicensed 60 GHz band from 57 GHz to 64 GHz, with a fractional -10 dB bandwidth of 11.6%.

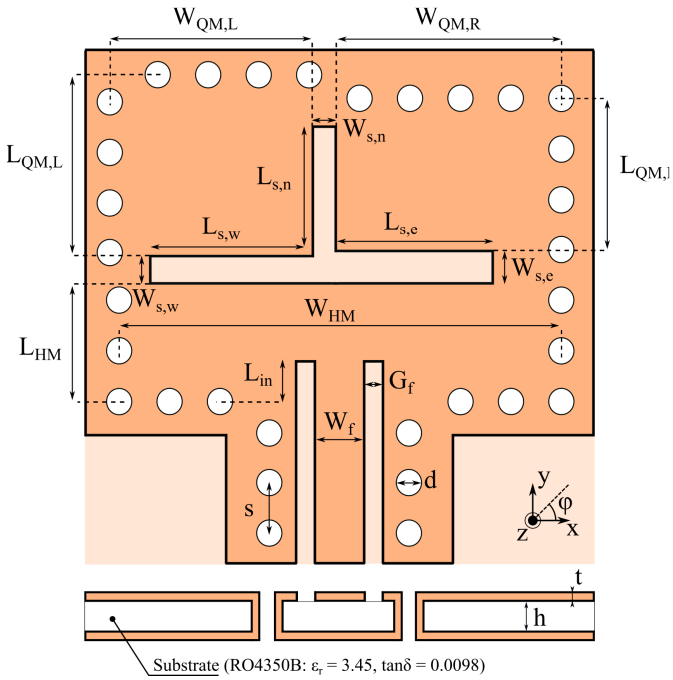

Fig. 8: Novel coupled HM- and QMSIW wideband antenna topology: three miniaturized cavity resonators are combined into a single antenna element.

TABLE I
DIMENSIONS FOR THE NOVEL COUPLED HM- AND QMSIW WIDEBAND ANTENNA TOPOLOGY

W_{HM}	1.92	$L_{s,e}$	0.68	L_{in}	0.56	*Dimensions (mm)*
L_{HM}	0.70	$W_{s,n}$	0.21	d	0.25	
$W_{QM,L}$	1.06	$L_{s,n}$	0.84	s	0.40	
$L_{QM,L}$	0.99	$W_{s,w}$	0.21	h	0.50	
$W_{QM,R}$	1.15	$L_{s,w}$	0.82	t	0.03	
$L_{QM,R}$	0.98	W_f	0.42	ε_r	3.45	
$W_{s,e}$	0.16	G_f	0.10	tanδ	0.0098	

The magnitude of the electric field inside the antenna at the three resonance frequencies is presented in Fig. 10. It is clear from Fig. 10 (a) that the electric field is dominant in the left QMSIW for the first resonance, which confirms the relation to

This article has been accepted for publication in a future issue of this journal, but has not been fully edited. Content may change prior to final publication. Citation information: DOI 10.1109/TAP.2017.2760360, IEEE Transactions on Antennas and Propagation

the resonances perceived in the reflection coefficient. Similarly, the electric fields at the second and third resonance frequency are dominant in the right QMSIW and the HMSIW, respectively. It is confirmed that the field distribution inside the HMSIW at its resonance frequency is very similar to half of the field distribution of a TE_{101}-mode in a full rectangular SIW cavity. Equivalently, the electric field inside the QMSIW is approximately equal to a quarter of the field of a TE_{101}-mode. Hence, it is proven that the SIW miniaturization technique, discussed in Section I, can be applied while maintaining performance. This will be further validated by means of measurements in Section IV.

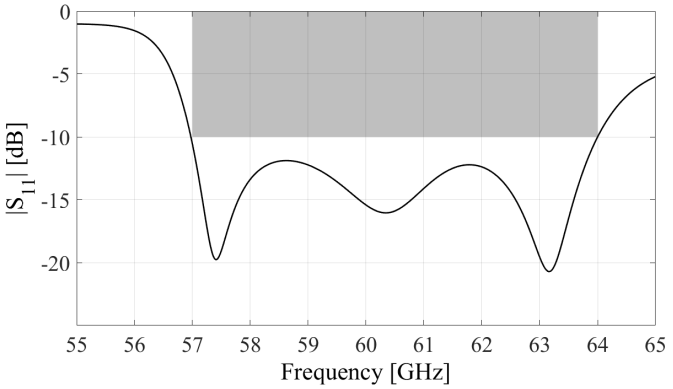

Fig. 9: Simulated reflection coefficient for the novel coupled HM- and QMSIW antenna: bandwidth enhancement by distributing three distinct resonance peaks over the 60 GHz band.

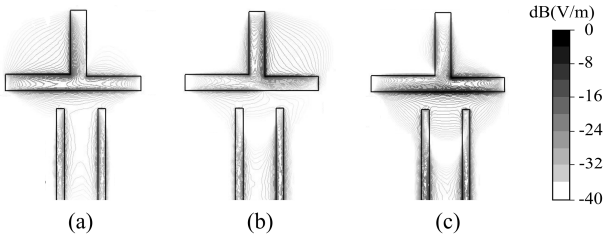

Fig. 10: Simulated normalized electric field distribution inside the antenna observed at the three resonance frequencies: (a) 57.5 GHz, (b) 60.4 GHz and (c) 63 GHz. (For clarity of the figure, the vias are not shown.)

C. *Antenna Far-Field Performance*

The gain in terms of bandwidth by coupling the resonators, as such distributing three resonances over the desired frequency range, is a significant novelty. A possible downside of this new topology, however, is the polarization, as discussed further in this section. Since slots are present in both the x- and y-directions, pure linear polarization is no longer achieved; hence the polarization is elliptical. Nonetheless, if we consider the far-field performance in light of the targeted application, i.e. 5G end user equipment, the obtained elliptical polarization may not be a significant drawback. The casing of the mobile device and the proximity of the user will inevitably affect the radiation pattern and cause depolarization, even for purely linearly or circularly polarized topologies [28]-[30]. Moreover, at any one of the individual resonances, the electric field is dominant in one of the three individual cavities. This will cause the main lobe direction to slightly tilt depending on frequency. Nonetheless, it is shown here and in Section IV that the main lobe only varies within a limited angular region of the 3dB-beam width.

The simulated antenna directivity and gain in the z-direction as a function of frequency are presented in Fig. 11. The simulated directivity and gain are higher than 7 dBi and 5 dBi, respectively, and very stable across the entire bandwidth of the antenna.

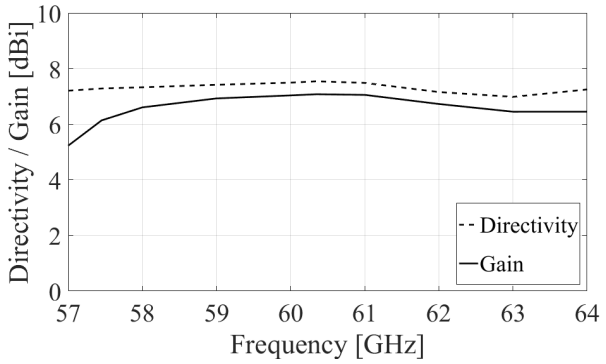

Fig. 11: Simulated directivity and gain of the antenna in the z-direction as a function of frequency.

The simulated radiation patterns at the three resonant frequencies are presented in Fig. 12. As different cavity resonances are dominant with respect to frequency, the E-planes become frequency-dependent and are accordingly defined as $\varphi = 135°$, 45° and 90° for the resonance in the left QMSIW, right QMSIW and HMSIW, respectively. Similarly, the corresponding H-planes are defined as $\varphi = 45°$, 135° and 0°. A 3 dB beam width of more than 80 degrees and a maximum antenna directivity of 7.53 dBi are achieved. As already discussed in Section II, the loss in radiation pattern purity is a minor drawback of this novel antenna topology. As is clear from Fig. 12, the main beam direction is slightly frequency dependent. Nevertheless, the variation of the beam is confined within the angular region of the 3 dB beam width; hence the frequency dependency has no significant impact on the far-field performance of the antenna. In addition, pure linear polarization is no longer achieved. As illustrated by the relatively high cross-polarization levels in Fig. 12, the antenna is elliptically polarized.

III. Manufacturing Process

An additional benefit of the coupled HM- and QMSIW topology is the cost efficiency and the straightforward design process. The antenna is manufactured on a single-layer substrate using the RF-pool fabrication process at Eurocircuits [31], which is a standard PCB manufacturing technology. Hence, the fabrication is low-cost, repeatable and it guarantees a high yield, given a thorough understanding of the fabrication process.

A. *Fabrication tolerances*

One of the key challenges of antenna design at millimeter-wave (mmWave) frequencies is coping with the fabrication

This article has been accepted for publication in a future issue of this journal, but has not been fully edited. Content may change prior to final publication. Citation information: DOI 10.1109/TAP.2017.2760360, IEEE Transactions on Antennas and Propagation

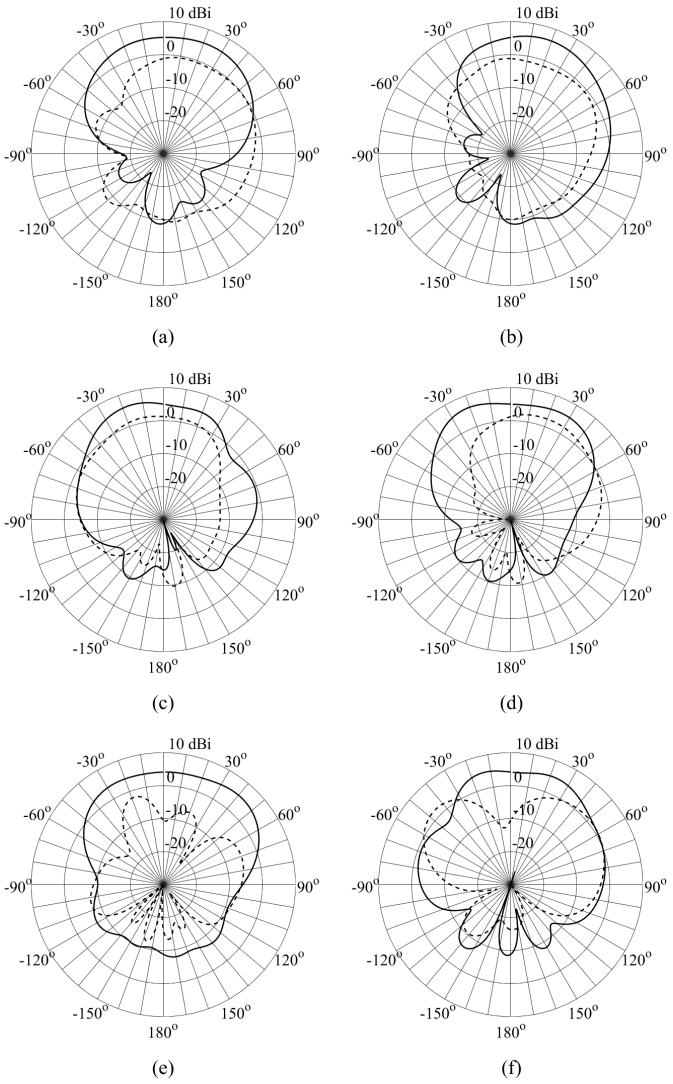

Fig. 12: Simulated radiation pattern (directivity) of co-polarization (solid lines) and cross-polarization (dashed lines): for the first resonance at 57.5 GHz (a) in the φ = 135° plane and (b) φ = 45° plane. For the second resonance at 60 GHz (c) in the φ = 45° plane and (d) φ = 135° plane, and for the third resonance at 63 GHz (e) in the φ = 90° plane and (f) φ = 0° plane.

accuracy and tolerances [32], e.g., the variations on the via diameter and placement for SIW technology need to be considered carefully. To arrive at a robust design, fabrication errors have to be taken into account throughout the early design stages, e.g., by means of a corner analysis. As the free-space wavelength at 60 GHz is only 5 mm, the effects of fabrication inaccuracies become more pronounced.

Design analyses of the proposed SIW antenna have revealed that the diameter of the vias and the thickness of the Cu cladding are critical parameters in terms of antenna performance. If, e.g., the via diameter for a fabricated prototype is larger than expected, the effective length and width of the cavities become smaller, shifting the resonances to higher frequencies. To assess the extent of potential fabrication errors, several test boards with via holes were manufactured and their cross-sections evaluated, as depicted in Fig. 13. Measurements have revealed that the via diameter and Cu thickness have a worst-case variation of ±10 µm and ±5 µm, respectively, serving as a basis for the corner analysis performed in Section III.D.

B. Material characterization

Material characteristics, such as ε_r and tanδ, of high frequency laminates are commonly only specified up to 40 GHz. At extremely high frequencies such as 60 GHz, one can safely assume that the substrate parameters diverge from those values [33]. Therefore, a method for material characterization based on resonant SIW cavities [34] is exploited to obtain the values for both ε_r and tanδ as a function of frequency. It is determined that ε_r = 3.45 and tanδ = 0.0098 at 60 GHz.

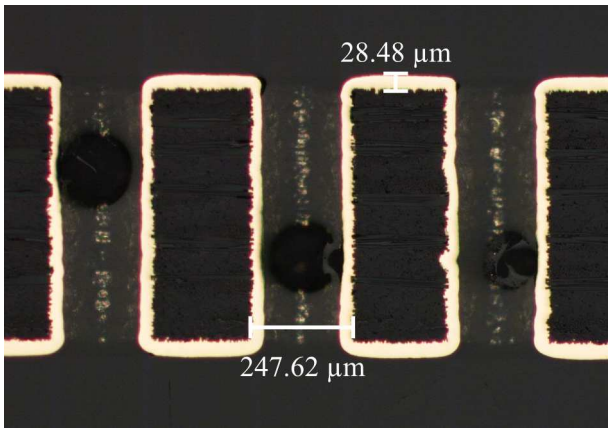

Fig. 13: Via-hole cross-section for evaluation of fabrication errors.

C. Loss mechanisms

At mmWave frequencies, a good understanding of the pertinent loss mechanisms is a prerequisite for an efficient and robust antenna design. Substrate and metal losses increase significantly with frequency. They need be taken into account in the early design stages, to minimize the number of design iterations and improve the overall performance. For the novel HMSIW-QMSIW topology, the parameters of the substrate material have been experimentally determined as described in Section III.B. An average surface roughness of the copper cladding of 3.1 µm has been extracted from the cross-section presented in Section III.A, which corresponds with the value of 2.8 µm in the datasheet of the Rogers laminate. As the skin depth at 60 GHz is smaller than 300 nm, a high copper surface roughness can be a source for significant additional losses. The aforementioned extracted parameters and surface roughness are included in the full-wave simulation model of the antenna and the different loss mechanisms are analyzed.

The simulated power losses in the substrate and metal cladding are depicted in Fig. 14. It is clear that the substrate losses are dominant over the losses in the copper cladding, which is to be expected when considering the relatively large substrate height of the SIW antenna topology [35][36]. Nevertheless, as this effect is accounted for during the design stage, the simulation model provides an adequate prediction of a realistic antenna prototype.

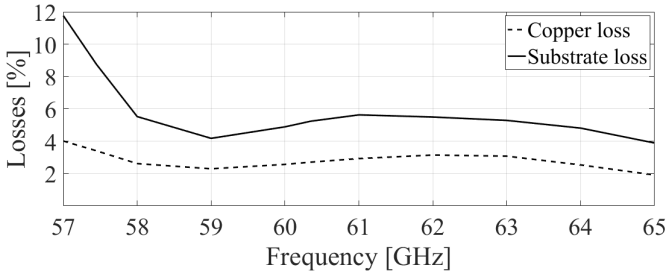

Fig. 14: Simulated power loss in the substrate material (solid line) and copper cladding (dashed line) as a function of frequency.

D. Corner analysis

In Section III.A, the fabrication tolerances on the critical design parameters are determined by studying cross sections. The extracted value of ±10 µm and ±5 µm for the tolerances on the via diameter and copper cladding thickness, respectively, are the basis for the simulation-based corner analysis depicted in Fig. 15 and Fig. 16.

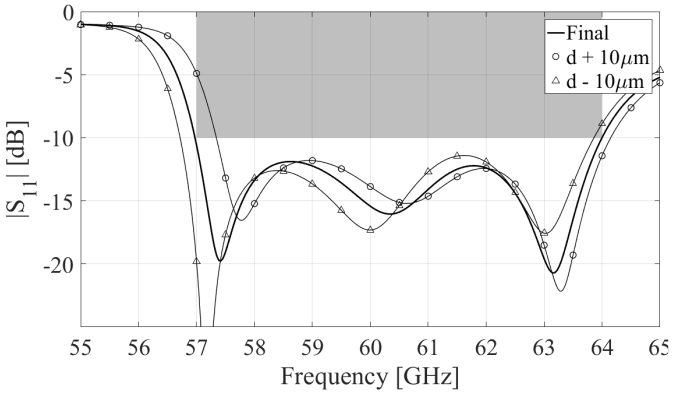

Fig. 15: Effect of fabrication errors on via diameter: final design (solid line), d + 10µm (circle marker) and d - 10µm (triangle marker).

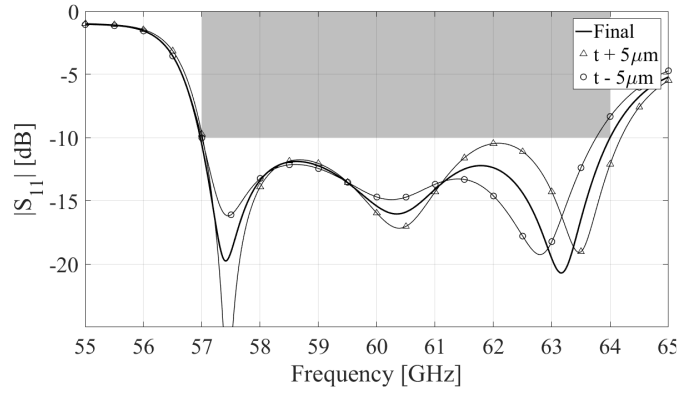

Fig. 16: Effect of fabrication errors on copper cladding thickness: final design (solid line), t + 5µm (triangle marker) and t - 5µm (circle marker).

To assess the effects of other possible fabrication errors, e.g. misalignment of the via rows, and the consequential errors on the dimensions of these three coupled SIW cavities composing the antenna, a parametric study is performed. The simulated reflection coefficient for a 50 µm error on the length of the left QMSIW is shown in Fig. 17. The first resonance, at 57.5 GHz, shifts due to an error on the length of the left QMSIW. A variation of only 50 µm substantially modifies the resonance frequency. Similar results are obtained for the right QMSIW and HMSIW with the second and third resonance, respectively.

The amount of coupling between the three resonant cavities depends on the width of the slots. Fig. 18 shows the effect of a 25 µm error on $W_{s,e}$, which determines the coupling between the second resonance in the right QMSIW and the third resonance in the HMSIW. An increase in slot width between two adjacent cavities decreases coupling, separating the two corresponding cavity resonances further in terms of frequency. When the slot between the right QMSIW and the HMSIW widens by 25 µm, the second and third resonance frequencies are further separated, as illustrated in Fig. 18. When the slot width decreases, the capacitive coupling increases and the cavity resonances merge. Similar results are obtained for errors on $W_{s,w}$ and $W_{s,n}$.

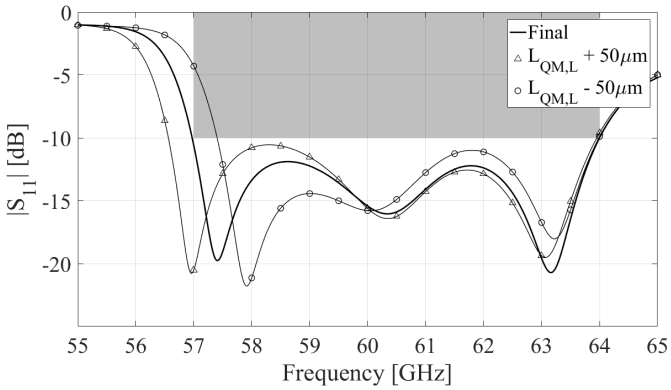

Fig. 17: Effect of fabrication errors on the coupled cavities' dimensions: final design (solid line), $L_{QM,L}$ + 50µm (triangle marker) and $L_{QM,L}$ - 50µm (circle marker).

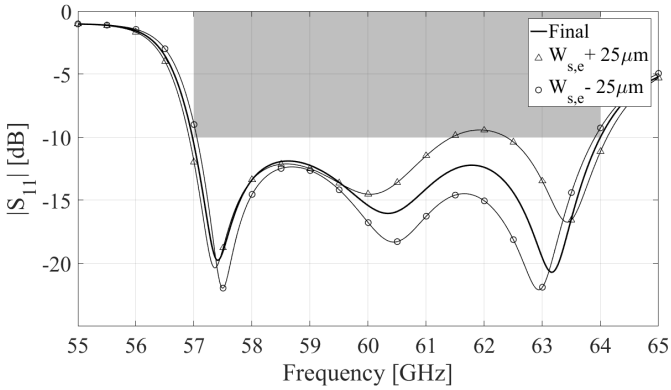

Fig. 18: Effect of fabrication errors on slot widths: final design (solid line), $W_{s,e}$ + 25µm (triangle marker) and $W_{s,e}$ - 25µm (circle marker).

Fig. 19 shows the effect of a 25 µm fabrication error on the slot length $L_{s,e}$, separating the right QMSIW and the HMSIW cavity. When the slot length $L_{s,e}$ increases, the coupling increases and the second and third resonance further merge. When the length of the slot decreases, the resonance frequencies are driven further apart. Similar results are obtained for the slot lengths $L_{s,w}$ and $L_{s,n}$.

The RO4350B laminate's relative permittivity, extracted in Section III.B, is $\varepsilon_r = 3.45$ at 60 GHz. Fig. 20 shows a shift by

This article has been accepted for publication in a future issue of this journal, but has not been fully edited. Content may change prior to final publication. Citation information: DOI 10.1109/TAP.2017.2760360, IEEE Transactions on Antennas and Propagation

approximately 500 MHz for a deviation of 1.5%, being $\varepsilon_r \pm 0.05$. Hence, a robust and reliable method needs to be applied to ensure a highly accurate estimate of the substrate characteristics, as performed in Section III.B.

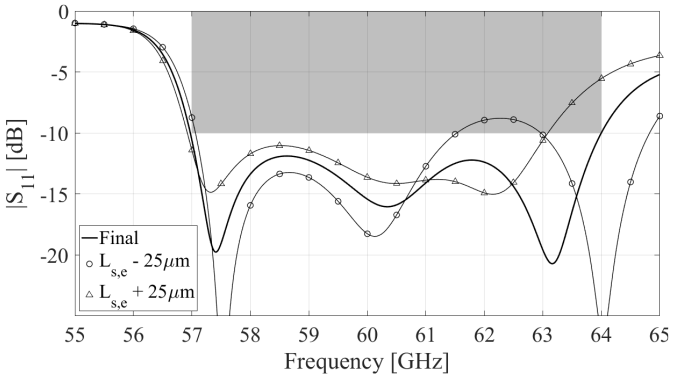

Fig. 19: Effect of fabrication errors on slot lengths: final design (solid line), $L_{s,e}$ + 25µm (triangle marker) and $L_{s,e}$ - 25µm (circle marker).

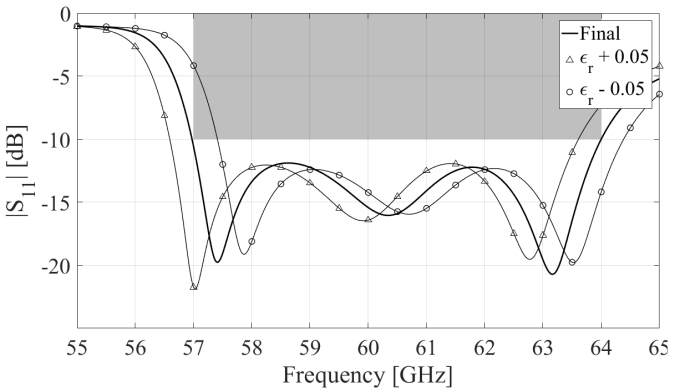

Fig. 20: Sensitivity of impedance bandwidth to relative permittivity: final design (solid line), ε_r + 0.05 (triangle marker) and ε_r - 0.05 (circle marker).

IV. Experimental Validation

A prototype of the novel coupled HMSIW and QMSIW antenna, fabricated with dimensions as presented in Table I, is shown in Fig. 21. Compared to the simulation model, a second row of plated vias was added along the circumference of the antenna to further eliminate leakage of the electromagnetic fields along the substrate. This is a purely precautionary measure, to cope with variations in the spacing between the vias as a result of fabrication tolerances. The additional row of vias does not affect the performance of the antenna in any regard.

The reflection coefficient of the fabricated prototype was measured using a Keysight N5247A PNA-X Microwave Network Analyzer and solder-free V-type (1.85 mm) End-Launch connectors by Southwest Microwave [37]. The coaxial pin of the connectors is not soldered, but press-fit onto the signal trace of the PCB. To compensate for the additional capacitance generated by the interference fit, the signal trace is tapered and optimized to add inductance.

A Thru-Reflect-Line (TRL) calibration kit [38] was designed and exploited to de-embed the connector and feed line, as such positioning the port reference plane closer to the antenna. This allows for an adequate comparison between simulated and measured S-parameters. The simulated and measured reflection coefficients, w.r.t. 50 Ω, of the novel 60 GHz coupled HM- and QMSIW antenna are depicted in Fig. . A measured -10 dB fractional impedance bandwidth of 11.7% (7 GHz) is obtained, in excellent agreement with simulations.

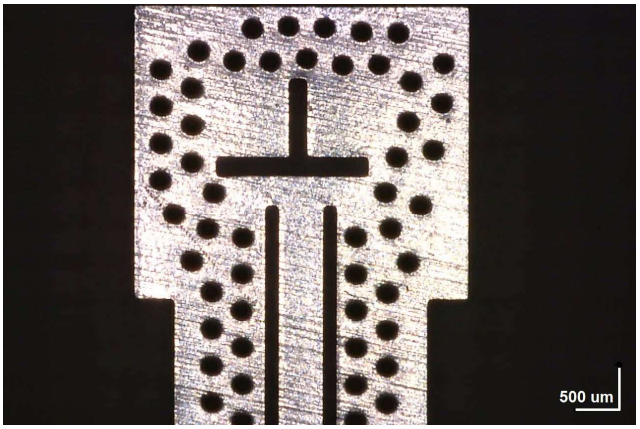

Fig. 21: Fabricated prototype of the novel 60 GHz coupled HMSIW- QMSIW antenna.

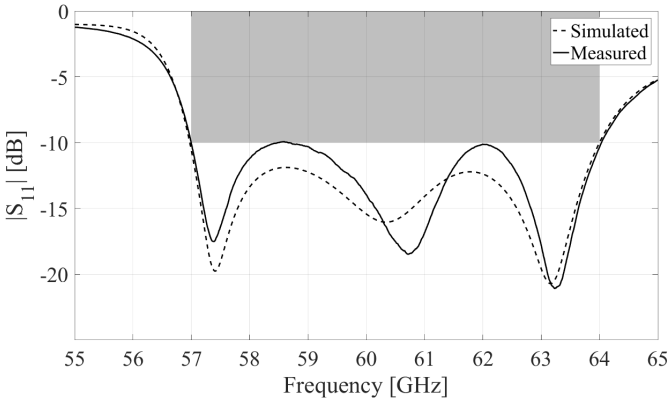

Fig. 22: Reflection coefficient of the fabricated coupled HM- and QMSIW antenna prototype: measured (dashed line) versus simulated (solid line).

The far-field performance of the antenna prototype was measured in the mm-Wave Anechoic Chamber (MMWAC) [39] at the Eindhoven University of Technology (TUe). This fully automated system consists of an anechoic chamber with a 1 meter diameter and 0.5 m height. The measurement setup is operational in the frequency range from 50 GHz up to 90 GHz and can measure antenna prototypes with a maximum gain up to 23 dBi at 60 GHz. The antenna-under-test (AUT) is mounted on a translation table. A microscope camera ensures accurate phase center alignment with respect to the reference antenna and positioning of the GSG probe to excite the AUT. Owing to the three rotational axes along which the reference antenna can be positioned, a hemispherical radiation pattern of an AUT can be measured.

Cross-sections of the measured and simulated radiation patterns of the antenna are shown in Fig. 23 for the first resonance in the left QMSIW, in Fig. 24 for the second

TABLE II
COMPARISON OF THIS WORK WITH REPORTED WIDEBAND 60 GHZ ANTENNA TOPOLOGIES

	[4]	[16]	[18]	[25]	[26]	This work
Topology	SIW slot array	SIW slot array	Dual resonant slot and patch array	Stacked patch array	SIW wide slot array	Coupled SIW cavities
Technology	PCB	PCB	LTCC	PCB	PCB	PCB
Frequency	60 GHz	60 GHz	60 GHz	79 GHz	60 GHz	60 GHz
Stack thickness	0.56 mm	0.79 mm	1.1 mm	0.68 mm	0.635 mm	0.56 mm
No. of layers	1	1	3	7	1	1
No. of elements		64	4	2	8	1
Dimensions	-	35.0 x 56.4 x 0.79 mm^3	9.7 x 6.5 x 1.1 mm^3	1.27 x 1.35 x 0.68 mm^3	27.0 x 15.5 x 0.635 mm^3	3.7 x 3.3 x 0.56 mm^3
Bandwidth	3.8 %	18.3 %	23.3 %	9.7 %	11.5 %	12 %
Gain	13.5 dBi	21 dBi	9 dBi	5.2 dBi	12 dBi	6.32 dBi
Efficiency	68 %	-	-	75 %	-	68 %

resonance in the right QMSIW, and in Fig. 25 for the third resonance in the HMSIW. A good agreement between simulated and measured results is achieved. The simulation model includes the GSG measurement probe as well as the mount for the antenna under test, as their influence on the measured radiation pattern is not negligible at mmWave [40]-[41]. As such, all parasitic radiation and reflections are included in the simulation and the experimental setup is approximated as close as possible. The overetching of the copper cladding, surface roughness and hollow vias are taken into account to accurately model the fabricated prototype. Moreover, the break faces at the edges of the PCB are included in the simulation as their influence on the diffraction pattern is no longer negligible at mmWave.

The broadside total gain values are calculated at all three resonance frequencies of the coupled HM- and QMSIW antenna prototype. Table III summarizes the measurement results and compares them to simulated values. Again, a good agreement between simulated and measured results is achieved. Moreover, the measured broadside antenna gain is larger than 5.1 dBi, and fairly constant, within the entire 7 GHz impedance bandwidth.

TABLE III
SIMULATED AND MEASURED BROADSIDE GAIN AND RADIATION EFFICIENCY AT THE THREE RESONANCE FREQUENCIES OF THE FABRICATED ANTENNA PROTOTYPE

Frequency	Gain		Radiation efficiency	
	Sim.	Meas.	Sim.	Meas.
57.5 GHz	5.80 dBi	5.92 dBi	64.3 %	65.8 %
61 GHz	6.45 dBi	6.32 dBi	69.3 %	67.7 %
63 GHz	5.16 dBi	5.14 dBi	67.8 %	67.5 %

As shown in Table III the measured radiation efficiency is larger than 65 % over the entire impedance bandwidth, with a maximum of 67.7 % at the second resonance in the right QMSIW cavity.

Table II compares the measured performance of the novel 60 GHz coupled HM- and QMSIW antenna to other reported topologies. It is clear that the topology advocated in this work achieves a rather large impedance bandwidth, despite the low-profile single substrate layer design, while maintaining a small footprint, a low profile and compatibility to cost-efficient standard PCB processing. Keeping in mind the envisioned deployment in end user equipment, it is evident that trade-offs have been made to find good balance between large impedance bandwidth and ease of integration.

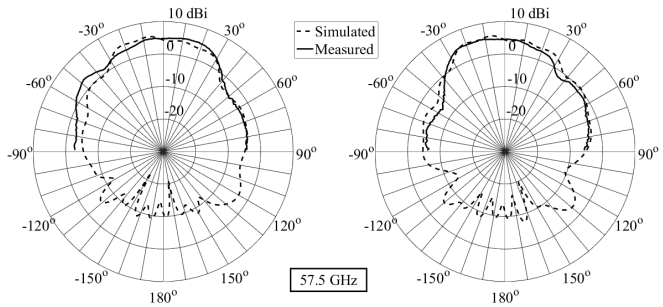

Fig. 23: Measured and simulated total gain radiation pattern of the antenna prototype at resonance in left QMSIW: (a) E-plane at φ = 135°, (b) H-plane at φ =45°.

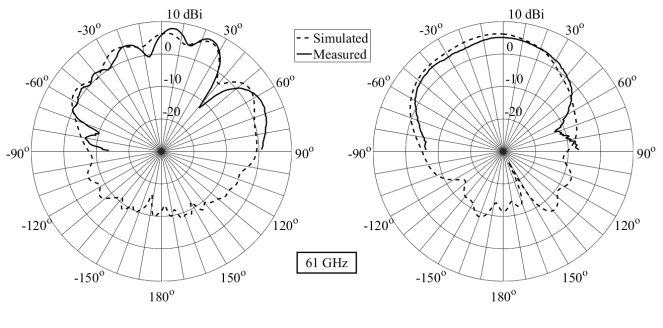

Fig. 24: Measured and simulated radiation pattern of the antenna prototype at resonance in right QMSIW: (a) E-plane at φ = 45°, (b) H-plane at φ = 135°.

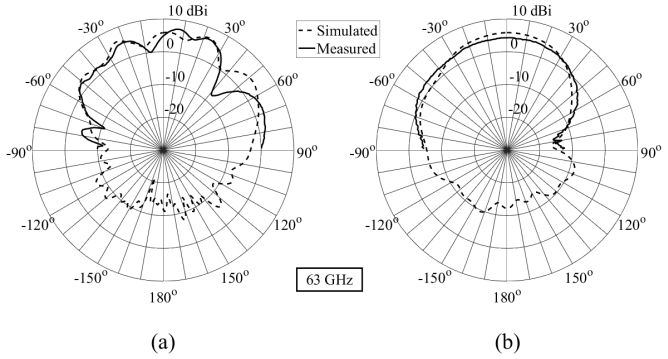

Fig. 25: Measured (dashed line) and simulated (solid line) radiation pattern of the antenna prototype at resonance in HMSIW: (a) E-plane at φ = 90°, (b) H-plane at φ = 0°.

V. CONCLUSIONS

A novel wideband SIW antenna topology based on coupled resonators has been designed and validated for operation in the [57-64] GHz IEEE 802.11ad band. By exploiting a miniaturization technique, three antenna elements are combined into a footprint of about half a wavelength. Through tight coupling between the separate resonant cavities, their resonances are distributed over the frequency band of operation such that the impedance bandwidth is significantly enhanced. This large bandwidth is achieved without any trade-off in terms of footprint or cost, as the design is compatible with standard two-layer PCB manufacturing processes. A measured fractional impedance bandwidth of 11.7% (7 GHz) is obtained. The measured broadside antenna gain is larger than 5.1 dBi over the entire impedance bandwidth and a measured radiation efficiency of more than 65% is obtained.

The shielding capabilities of the SIW technology confine the electromagnetic fields within the cavities, prohibiting propagation of surface waves. Hence, the novel HM- and QMSIW antenna is ideal for close integration in compact antenna arrays.

When placing the advocated topology in a 4-element uniform linear array configuration with an inter-element spacing of half a wavelength, full-wave simulations show that the mutual coupling remains below -18 dB for adjacent elements and below -25 dB for non-adjacent elements in the entire frequency range from 57-64 GHz. Therefore, it is straightforward to deploy the proposed antenna topology in an array configuration to achieve a higher gain.

ACKNOWLEDGMENT

The authors would like to thank the ERC for the advanced grant 695495 “ATTO: A new concept for ultra-high capacity wireless networks” and Lothar Mader for performing the cross-sections on the via hole test structures for the assessment of the fabrication tolerances. Part of this work was supported by BELSPO through the IAP Phase VII BESTCOM project.

REFERENCES

[1] P. Smulders, “Impact of regulations on feasible distance between 60 GHz devices,” in *2010 Proceedings of the Fourth European Conference on Antennas and Propagation (EuCAP),* 2010, pp. 1-4.

[2] A. Deshmukh and S. Bodhe, “Characterization of radio propagation at 60 GHz channel," in *First Asian Himalayas International Conference on Internet (AH-ICI)*, Nov 2009, pp. 1-8.

[3] M. Bozzi, A. Georgiadis and K. Wu, "Review of substrate-integrated waveguide circuits and antennas," *IET Microwaves, Antennas & Propagation*, vol. 5, no. 8, pp. 909-920, June 6 2011.

[4] F. F. He, K. Wu, W. Hong, L. Han and X. P. Chen, "Low-Cost 60-GHz Smart Antenna Receiver Subsystem Based on Substrate Integrated Waveguide Technology," *IEEE Transactions on Microwave Theory and Techniques*, vol. 60, no. 4, pp. 1156-1165, April 2012.

[5] N. Tiwari and T. R. Rao, "A switched beam antenna array with butler matrix network using substrate integrated waveguide technology for 60 GHz communications," *2015 International Conference on Advances in Computing, Communications and Informatics (ICACCI),* Kochi, 2015, pp. 2152-2157.

[6] S. Lemey, T. Castel, P. Van Torre, T. Vervust, J. Vanfleteren, P. Demeester, D. Vande Ginste, H. Rogier, "Threefold Rotationally Symmetric SIW Antenna Array for Ultra-Short-Range MIMO Communication," *IEEE Transactions on Antennas and Propagation*, vol. 64, no. 5, pp. 1689-1699, May 2016.

[7] K. K. Samanta, D. Stephens and I. D. Robertson, "Design and performance of a 60-GHz multi-chip module receiver employing substrate integrated waveguides," *IET Microwaves, Antennas & Propagation*, vol. 1, no. 5, pp. 961-967, October 2007.

[8] K. Kuhlmann and A. F. Jacob, "Active 30 GHz antenna array for digital beamforming and polarization multiplexing," *2010 IEEE MTT-S International Microwave Symposium Digest (MTT)*, Anaheim, CA, 2010, pp. 1276-1279.

[9] F. Giuppi, A. Georgiadis, A. Collado and M. Bozzi, "Active substrate integrated waveguide (SIW) antenna with phase-shifterless beam-scanning capabilities," *2012 IEEE MTT-S International Microwave Symposium Digest (MTT)*, Montreal, QC, Canada, 2012, pp. 1-3.

[10] H. Rogier, S. Agneessens, T. Castel, S. Lemey, F. Declercq, P. Vanveerdeghem, P. Van Torre, L. Vallozzi, W. Joseph, "Novel wearable antenna systems for high datarate mobile communication in healthcare," *2014 EAI 4th International Conference on Wireless Mobile Communication and Healthcare (Mobihealth)*, Athens, 2014, pp. 188-191.

[11] F. Giuppi, A. Georgiadis, A. Collado, M. Bozzi and L. Perregrini, "Tunable SIW cavity backed active antenna oscillator," *Electronics Letters*, vol. 46, no. 15, pp. 1053-1055, July 22 2010.

[12] S. Agneessens and H. Rogier, "Compact Half Diamond Dual-Band Textile HMSIW On-Body Antenna," *IEEE Transactions on Antennas and Propagation*, vol. 62, no. 5, pp. 2374-2381, May 2014.

[13] O. Caytan, S. Lemey, S. Agneessens, D. Vande Ginste, P. Demeester,C. Loss, R. Salvado and H. Rogier, "Half-Mode Substrate-Integrated-Waveguide Cavity-Backed Slot Antenna on Cork Substrate," *IEEE Antennas and Wireless Propagation Letters*, vol. 15, no. , pp. 162-165, 2016.

[14] C. Jin, R. Li, A. Alphones and X. Bao, "Quarter-Mode Substrate Integrated Waveguide and Its Application to Antennas Design," *IEEE Transactions on Antennas and Propagation*, vol. 61, no. 6, pp. 2921-2928, June 2013.

[15] Q. Wu, H. Wang, C. Yu and W. Hong, "Low-Profile Circularly Polarized Cavity-Backed Antennas Using SIW Techniques," *IEEE Transactions on Antennas and Propagation*, vol. 64, no. 7, pp. 2832-2839, July 2016.

[16] S. Liao, P. Chen, P. Wu, K. M. Shum and Q. Xue, "Substrate-Integrated Waveguide-Based 60-GHz Resonant Slotted Waveguide Arrays With Wide Impedance Bandwidth and High Gain," *IEEE Transactions on Antennas and Propagation*, vol. 63, no. 7, pp. 2922-2931, July 2015.

[17] J. Pourahmadazar and T. A. Denidni, "High Gain Substrate Integrated Waveguide Resonant Slot Antenna Array for mm-Wave Band Radio," *2015 IEEE International Conference on Ubiquitous Wireless Broadband (ICUWB)*, Montreal, QC, 2015, pp. 1-4.

[18] K. S. Chin, W. Jiang, W. Che, C. C. Chang and H. Jin, "Wideband LTCC 60-GHz Antenna Array With a Dual-Resonant Slot and Patch Structure," *IEEE Transactions on Antennas and Propagation*, vol. 62, no. 1, pp. 174-182, Jan. 2014.

[19] H. Jin, W. Che, K. S. Chin, G. Shen, W. Yang and Q. Xue, "60-GHz LTCC Differential-Fed Patch Antenna Array With High Gain by Using Soft-Surface Structures," *in IEEE Transactions on Antennas and Propagation*, vol. 65, no. 1, pp. 206-216, Jan. 2017.

[20] S. Liao and Q. Xue, "Dual Polarized Planar Aperture Antenna on LTCC for 60-GHz Antenna-in-Package Applications," *in IEEE Transactions on Antennas and Propagation*, vol. 65, no. 1, pp. 63-70, Jan. 2017.

[21] J. Xu, Z. N. Chen, X. Qing and W. Hong, "Bandwidth Enhancement for a 60 GHz Substrate Integrated Waveguide Fed Cavity Array Antenna on LTCC," in *IEEE Transactions on Antennas and Propagation*, vol. 59, no. 3, pp. 826-832, March 2011.

[22] S. B. Yeap, Z. N. Chen and X. Qing, "Gain-Enhanced 60-GHz LTCC Antenna Array With Open Air Cavities," *IEEE Transactions on Antennas and Propagation*, vol. 59, no. 9, pp. 3470-3473, Sept. 2011.

[23] D. G. Kam, D. Liu, A. Natarajan, S. Reynolds, H. C. Chen and B. A. Floyd, "LTCC Packages With Embedded Phased-Array Antennas for 60 GHz Communications," *IEEE Microwave and Wireless Components Letters*, vol. 21, no. 3, pp. 142-144, March 2011.

[24] L. Wang, Y. X. Guo and W. Wu, "Wideband 60 GHz circularly polarised stacked patch antenna array in low temperature co-fired ceramic technology," in IET Microwaves, Antennas & Propagation, vol. 9, no. 5, pp. 436-445, 2015.

[25] M. Mosalanejad, S. Brebels, I. Ocket, C. Soens and G. A. E. Vandenbosch, "Stacked patch antenna sub-array with low mutual coupling for 79 GHz MIMO radar applications," *2017 11th European Conference on Antennas and Propagation (EUCAP)*, Paris, France, 2017, pp. 190-194.

[26] K. Gong, Z. N. Chen, X. Qing, P. Chen and W. Hong, "Substrate Integrated Waveguide Cavity-Backed Wide Slot Antenna for 60-GHz Bands," *IEEE Transactions on Antennas and Propagation*, vol. 60, no. 12, pp. 6023-6026, Dec. 2012.

[27] *MicroWave Studio* [Online]. Available: www.cst.com

[28] J. S. Colburn, Y. Rahmat-Samii, M. A. Jensen and G. J. Pottie, "Evaluation of personal communications dual-antenna handset diversity performance," in *IEEE Transactions on Vehicular Technology*, vol. 47, no. 3, pp. 737-746, Aug 1998.

[29] A. L. Amadjikpe, D. Choudhury, G. E. Ponchak, B. Pan, Y. Li and J. Papapolymerou, "Proximity Effects of Plastic Laptop Covers on Radiation Characteristics of 60-GHz Antennas," in *IEEE Antennas and Wireless Propagation Letters*, vol. 8, no. , pp. 763-766, 2009.

[30] Y. Huo, X. Dong, W. Xu, "5G Cellular User Equipment: From Theory to Practical Hardware Design", *Computing Research Repository (CoRR)*, April 2017.

[31] Eurocircuits. (2015). *"RF pool" – all the benefits of pooling on RF materials* [Online]. Available: http://www.eurocircuits.com/rf-pool-all-the-benefits-of-pooling-on-rf-materials/

[32] C. Oikonomopoulos-Zachos and M. Martínez-Vázquez, "Effect of technological tolerances in the design of a 60 GHz LTCC antenna," *2010 IEEE Antennas and Propagation Society International Symposium*, Toronto, ON, Canada, 2010, pp. 1-4.

[33] M. D. Huang, M. H. A. J. Herben, A. C. F. Reniers and P. F. M. Smulders, "Causes of discrepancies between measurements and em simulations of millimeter-wave antennas [Measurements Corner]," in *IEEE Antennas and Propagation Magazine*, vol. 55, no. 6, pp. 139-149, Dec. 2013.

[34] R. Moro, S. Agneessens, H. Rogier, A. Dierck and M. Bozzi, "Textile Microwave Components in Substrate Integrated Waveguide Technology," *IEEE Transactions on Microwave Theory and Techniques*, vol. 63, no. 2, pp. 422-432, Feb. 2015.

[35] M. Bozzi, M. Pasian and L. Perregrini, "Modeling of losses in substrate integrated waveguide components," *2014 International Conference on Numerical Electromagnetic Modeling and Optimization for RF, Microwave, and Terahertz Applications (NEMO)*, Pavia, 2014, pp. 1-4.

[36] M. Bozzi, L. Perregrini and K. Wu, "Modeling of Conductor, Dielectric, and Radiation Losses in Substrate Integrated Waveguide by the Boundary Integral-Resonant Mode Expansion Method," in *IEEE Transactions on Microwave Theory and Techniques*, vol. 56, no. 12, pp. 3153-3161, Dec. 2008.

[37] Southwest Microwave, Inc. (2016). *1.85 mm (V) DC to 67.0 GHz Connectors* [Online]. Available: http://mpd.southwestmicrowave.com

[38] G. F. Engen and C. A. Hoer, "Thru-Reflect-Line: An Improved Technique for Calibrating the Dual Six-Port Automatic Network Analyzer," *IEEE Transactions on Microwave Theory and Techniques*, vol. 27, no. 12, pp. 987-993, Dec 1979.

[39] A. C. F. Reniers, Q. Liu, M. H. A. J. Herben and A. B. Smolders, "Review of the accuracy and precision of mm-wave antenna simulations and measurements," *2016 10th European Conference on Antennas and Propagation (EuCAP)*, Davos, Switzerland, 2016, pp. 1-5.

[40] A. C. F. Reniers, A. R. van Dommele, A. B. Smolders and M. H. A. J. Herben, "The Influence of the Probe Connection on mm-Wave Antenna Measurements," *IEEE Transactions on Antennas and Propagation*, vol. 63, no. 9, pp. 3819-3825, Sept. 2015.

[41] A. C. F. Reniers, A. R. van Dommele, M. D. Huang and M. H. A. J. Herben, "Disturbing effects of microwave probe on mm-Wave antenna pattern measurements," *The 8th European Conference on Antennas and Propagation (EuCAP 2014)*, The Hague, The Netherlands, 2014, pp. 161-164.

Thomas Deckmyn (S'17) was born in 1993. He received the M.Sc. degree in electrical engineering from Ghent University, Ghent, Belgium, in 2015.
Since then, he has been working as a Ph.D. Researcher at the IDLab-Electromagnetics Group of the department of Information Technology (INTEC) at Ghent University/IMEC.
His research activities focus on the design and implementation of mmWave antenna solutions for next-generation wireless systems.

Sam Agneessens (S'14-M'16) received the M.S. and PhD degrees in electrical engineering from Ghent University, Belgium, in 2011 and 2015. He is currently a postdoctoral fellow of Research Foundation-Flanders (FWO-V), and is affiliated with the IDLab-electromagnetic group of the department of Information technology (INTEC) and the Centre for Microsystems (CMST) at Ghent University/IMEC.

His research focuses on the design and realization of robust antenna systems for wearable applications and mmWave antenna-on-package and active antenna solutions for 5G systems.
He received the URSI Young Scientist Award at the 2014 URSI General Assembly and was awarded the 2014 Premium Award for Best Paper in IET Electronics Letters, and received an honorable mention in the Student Paper competition at the 2014 IEEE International Symposium on Antennas and Propagation and USNC-URSI Radio Science Meeting.

Ad C. F. Reniers was born in Eindhoven, The Netherlands, in 1968. He received the Bachelor's degree in electrical engineering from Fontys University of applied sciences, and is currently pursuing his Ph.D. degree at Eindhoven University of Technology (TU/e), Eindhoven, Netherlands.
From 1999 to 2009, he worked with TNO Industry and Technique in Eindhoven, on research projects, affiliated to antenna-based sensors, antenna miniaturization, RFID applications, and energy harvesting. Since 2009, he has been associated with the Electromagnetics Group, Department of Electrical Engineering, Eindhoven University of Technology as education and research employee. He has extensive engineering and research experience in the field of antenna design and antenna measurement. His research interests include antenna miniaturization for integrated millimeter wave communication and wireless power transfer.

Bart Smolders was born in Hilvarenbeek, the Netherlands in 1965. He received his M.Sc. and Ph.D. degree in Electrical Engineering from the Eindhoven University of Technology (TU/e) in 1989 and 1994, respectively. From 1989 to 1991, he worked as an IC Designer at FEL-TNO, The Hague. From 1994 to 1997, he was a Radar System Designer with Thales, the Netherlands. From 1997 to 2000, he was project leader of the Square Kilometer Array (SKA) with the Netherlands Foundation for Research in Astronomy (ASTRON). From 2000 to 2010, he has been with NXP (formerly Philips) Semiconductors, The Netherlands, responsible for the innovation in the RF business line. Since 2010, he is a full-time professor at the TU/e in the Electromagnetics Group with special interest in antenna systems and applications. He is junior-past chairman of the IEEE Benelux section and chairman of the NERG (Nederlands Radio- en Elektronica Genootschap). Next to his research activities, he is the dean of the Electrical Engineering department of the TU/e. Publication can be found in: https://www.tue.nl/en/employee/ep/e/d/ep-uid/19910474/ep-tab/4/

Maarten Cauwe (M) received a Degree in electronics engineering from Ghent University, Ghent, Belgium, and a Ph.D. degree from the Center for Microsystems Technology (CMST), imec and Ghent University. He is currently leading the Advanced Packaging Team at CMST, and is involved in several projects concerning substrate technologies, chip assembly, medical packaging, and chip embedding. The Advanced Packaging team is composed of four highly skilled engineers in the field of packaging, pcb manufacturing, first and second level assembly, testing and failure analysis. His past research work was focused on component embedding in printed circuit boards, where he was involved from the first exploratory projects (Hiding Dies, 2004-2006) until the commercial industrialization of this technology in the frame of the HERMES project (2008-2011). He recently coordinated a project on this topic in cooperation with the European Space Agency (PCESA, 2014-2016). Other activities involve implantable packaging and flexible electronics.

Dries Vande Ginste (SM'12) received the M.S. degree and the Ph.D. degree in electrical engineering from Ghent University, Gent, Belgium, in 2000 and 2005, respectively. He is currently an Associate Professor at the Department of Information Technology, Ghent University and a Guest Professor at imec. In June and July 2004, he was a Visiting Scientist at the Department of Electrical and Computer Engineering, University of Illinois at Urbana-Champaign (UIUC), IL, USA. From September to November 2011, he was a Visiting Professor at the EMC Group, Dipartimento di Elettronica, Politecnico di Torino, Italy. He has authored or co-authored over 150 papers in international journals and in conference proceedings. His research interests include computational electromagnetics, electromagnetic compatibility, signal and power integrity, and antenna design.
Dr. Vande Ginste was awarded the International Union of Radio Science (URSI) Young Scientist Award at the 2011 URSI General Assembly and Scientific Symposium, the Best Poster Paper Award at the 2012 IEEE Electrical Design of Advanced Packaging and Systems Symposium (EDAPS), the Best Paper Award at the 2013 IEEE Workshop on Signal and Power Integrity (SPI), the Best Paper Award at the 2013 IEEE International Conference on Electrical Performance of Electronic Packaging and Systems (EPEPS) and the Best Paper Award at the 2016 IEEE Electrical Design of Advanced Packaging and Systems Symposium (EDAPS). He served as the co-chair of the 2014 IEEE Workshop on Signal and Power Integrity. He is a Senior Member of the IEEE.

Hendrik Rogier was born in 1971. He received the M.Sc. and Ph.D. degrees in Electrical Engineering from Ghent University, Gent, Belgium, in 1994 and in 1999, respectively. He is a currently a Full Professor with the Department of Information Technology of Ghent University, Belgium, Guest Professor at imec, Ghent, Belgium, and Visiting Professor at the University of Buckingham, UK. From October 2003 to April 2004, he was a Visiting Scientist at the Mobile Communications Group of Vienna University of Technology. He authored and coauthored more than 140 papers in international journals and more than 160 contributions in conference proceedings. He is serving as an Associate Editor of IET Electronics Letters, of IET Microwaves, Antennas and Propagation, and of the IEEE Transactions on Microwave Theory and Techniques. He acts as the URSI Commission B representative for Belgium. Within the IEEE Microwave Theory and Techniques Society, he is a member of Technical Committee 24 on RFID technology and within the European Microwave Association, he is a member of the Governing Board of Topical Group MAGEO on Microwaves in Agriculture, Environment and Earth Observation. His current research interests are antenna systems, radiowave propagation, body-centric communication, numerical electromagnetics, electromagnetic compatibility and power/signal integrity.
Dr. Rogier was twice awarded the URSI Young Scientist Award, at the 2001 URSI Symposium on Electromagnetic Theory and at the 2002 URSI General Assembly. In addition, he received the 2014 Premium Award for Best Paper in IET Electronics Letters, the Best Paper Award 1st place 2016 IEEE MTT-S Topical Conference on Wireless Sensors and Sensor Networks (WiSNet), the Best Poster Paper Award at the 2012 IEEE Electrical Design of Advanced Packaging and Systems Symposium (EDAPS), the Best Paper Award at the 2013 IEEE Workshop on Signal and Power Integrity (SPI) and the Joseph Morrissey Memorial Award for the First best scientific paper at BioEM 2013. He is a Senior Member of the IEEE.